Cell Reports

Resource

iPSC-Based Compound Screening and *In Vitro* Trials Identify a Synergistic Anti-amyloid β Combination for Alzheimer's Disease

Graphical Abstract

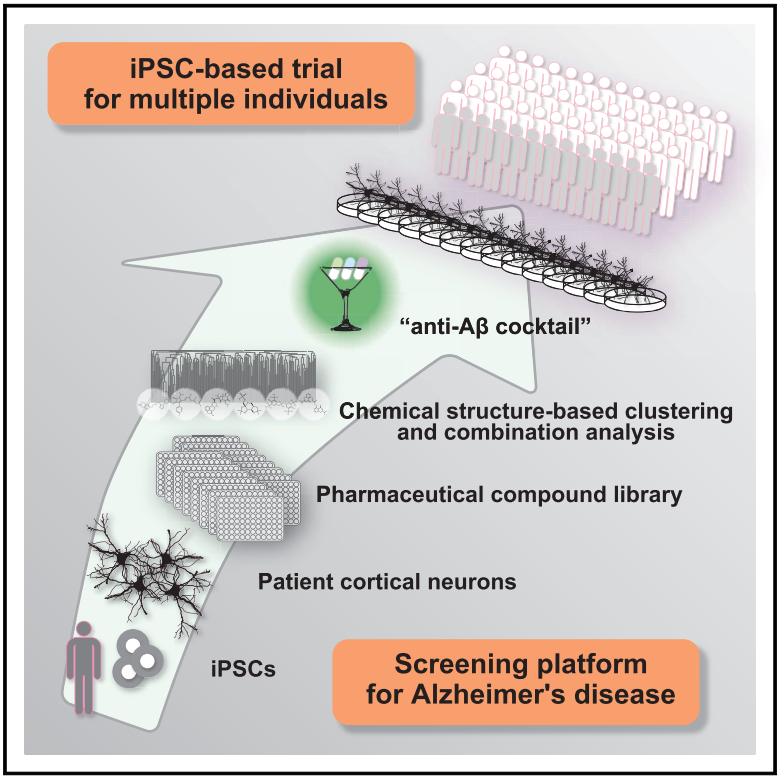

Highlights

- Rapid, robust neuronal induction from human iPSCs to model AD drug responsiveness
- iPSC-based screening of pharmaceutical compounds for Aβ phenotypes
- A combination of existing drugs synergistically improve Aβ phenotypes of AD
- Anti-Aβ cocktail decreases toxic Aβ levels in neurons derived from patients' cells

Authors

Takayuki Kondo, Keiko Imamura, Misato Funayama, ..., Ryuji Kaji, Nobuhisa Iwata, Haruhisa Inoue

Correspondence

haruhisa@cira.kyoto-u.ac.jp

In Brief

Kondo et al. used human iPSC-derived neurons, which offer human-specific drug responsiveness, for drug development for Alzheimer's disease (AD). Using iPSC-based screening of pharmaceutical compounds and chemical clustering, they found a combination of existing drugs that synergistically improve Aβ phenotypes of AD in cells.

Kondo et al., 2017, Cell Reports *21*, 2304–2312
November 21, 2017
https://doi.org/10.1016/j.celrep.2017.10.109

CellPress

OPEN ACCESS
CellPress

Cell Reports
Resource

iPSC-Based Compound Screening and *In Vitro* Trials Identify a Synergistic Anti-amyloid β Combination for Alzheimer's Disease

Takayuki Kondo,[1,2] Keiko Imamura,[1,2] Misato Funayama,[1] Kayoko Tsukita,[1] Michiyo Miyake,[1,2] Akira Ohta,[1] Knut Woltjen,[1,3] Masato Nakagawa,[1] Takashi Asada,[4] Tetsuaki Arai,[4] Shinobu Kawakatsu,[5] Yuishin Izumi,[6] Ryuji Kaji,[6] Nobuhisa Iwata,[7,8] and Haruhisa Inoue[1,2,9,*]

[1]Center for iPS Cell Research and Application (CiRA), Kyoto University, Kyoto 606-8507, Japan
[2]Drug-Discovery Cellular Basis Development Team, RIKEN BioResource Center, Kyoto 606-8507, Japan
[3]Hakubi Center for Advanced Research, Kyoto University, Kyoto 606-8501, Japan
[4]Department of Psychiatry, Division of Clinical Medicine, Faculty of Medicine, University of Tsukuba, Ibaraki 305-8575, Japan
[5]Department of Neuropsychiatry, Aizu Medical Center, Fukushima Medical University, Fukushima 969-3492, Japan
[6]Department of Clinical Neuroscience, Institute of Biomedical Sciences, Tokushima University Graduate School, Tokushima 770-8503, Japan
[7]Department of Genome-based Drug Discovery, Graduate School of Biomedical Sciences, Nagasaki University, Nagasaki 852-8521, Japan
[8]Unit for Dementia Research and Drug Discovery, Graduate School of Biomedical Sciences, Nagasaki University, Nagasaki 852-8521, Japan
[9]Lead Contact
*Correspondence: haruhisa@cira.kyoto-u.ac.jp
https://doi.org/10.1016/j.celrep.2017.10.109

SUMMARY

In the process of drug development, *in vitro* studies do not always adequately predict human-specific drug responsiveness in clinical trials. Here, we applied the advantage of human iPSC-derived neurons, which offer human-specific drug responsiveness, to screen and evaluate therapeutic candidates for Alzheimer's disease (AD). Using AD patient neurons with nearly 100% purity from iPSCs, we established a robust and reproducible assay for amyloid β peptide (Aβ), a pathogenic molecule in AD, and screened a pharmaceutical compound library. We acquired 27 Aβ-lowering screen hits, prioritized hits by chemical structure-based clustering, and selected 6 leading compounds. Next, to maximize the anti-Aβ effect, we selected a synergistic combination of bromocriptine, cromolyn, and topiramate as an anti-Aβ cocktail. Finally, using neurons from familial and sporadic AD patients, we found that the cocktail showed a significant and potent anti-Aβ effect on patient cells. This human iPSC-based platform promises to be useful for AD drug development.

INTRODUCTION

Human induced pluripotent stem cell (iPSC) technology has revolutionized drug discovery research (Shi et al., 2016) by making it possible to produce diseased cells from patients *in vitro*. In the research field of neurological diseases, direct biopsy of affected tissues from patients causes irreversible injury; therefore, cellular and animal models generated by the transduction and overexpression of disease-causative genes have been widely used for drug discovery research. However, recent studies have elucidated a large difference in drug responsiveness between human iPSC-derived cells and cancer cell lines (Liu et al., 2014; Mertens et al., 2013; Paull et al., 2015; Yahata et al., 2011). In the process of drug development, the total success rate from hit compounds to final launch is nearly 4.1%, according to some estimates (Paul et al., 2010), and is only 11.6% at clinical trial stages, even after successful preclinical studies. The cause of these low success rates in drug development may, at least partially, be attributed to a difference in drug responsiveness between human beings and other model animals and/or various drug dosages and transgenes that mimic the disease conditions. To minimize this gap, patient-derived iPSCs could be a promising resource for pharmacological research. Here, we modified direct conversion technology (Szabo et al., 2010; Zhang et al., 2013) for neuronal cells from human iPSCs (induced neurons: iNs) and achieved a neuronal cell culture with nearly 100% purity after only a 1-week differentiation period from iPSCs. This extremely pure and rapid method of neuronal differentiation can eliminate the variant efficiency of differentiation among iPSC clones (Onder and Daley, 2012; Thatava et al., 2013) and is more suitable for modeling a pathological condition and compound screening.

We applied this differentiation method to compound screening for Alzheimer's disease (AD), the most common cause of elderly dementia. One of the neuropathological hallmarks of AD is the formation of extracellular amyloid plaques that are composed of aggregated amyloid β peptides (Aβs) (Powers, 1997; Selkoe, 2004). Extensive studies of human genetics, neuropathology, and model animals indicate that the accumulation of Aβs is a triggering event that initiates a long-term pathological cascade of AD and eventually leads to dementia (Hardy and Selkoe, 2002; Selkoe, 2002). Aβ is produced by sequential cleavages of amyloid precursor protein (APP) by β-site APP cleaving enzyme 1 (BACE1) and γ-secretase, and these two enzymes have been

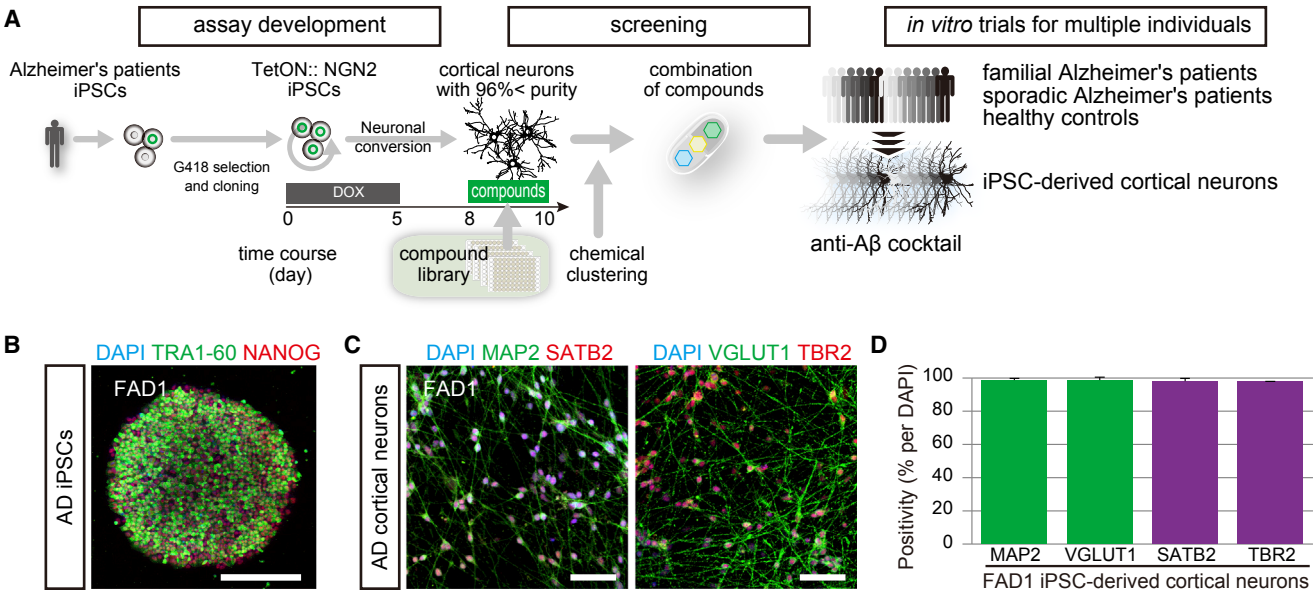

Figure 1. Transient NGN2 Expression Converts iPSCs into Cortical Neurons

(A) Schema of the differentiation system for iPSC-derived cortical neurons by using the *piggyBac* vector coding human *NGN2* gene, the compound-screening platform, and the *in vitro* trials.

(B) A generated FAD1-iPSC line expressed the pluripotency markers TRA1-60 (green) and NANOG (red). Scale bar, 200 μm.

(C) Day 8 FAD1 neurons expressed excitatory cortical neuron markers. Left: MAP2 (green) and SATB2 (red). Right: VGLUT1 (green) and TBR2 (red). Scale bars, 200 μm.

(D) Purity of day 8 neurons.

Data indicate mean ± SD (n = 3 for each clone).

the most important targets for disease-modifying drugs of AD. However, strong inhibition of γ-secretase widely perturbs the processing of numerous endogenous substrates important for physiological functions other than APP, and it has caused serious side effects after long-term treatment (Filser et al., 2015). After the failure in recent clinical trials of γ-secretase inhibitor, mainly due to on-target side effects in humans (De Strooper, 2014), BACE1 was considered as a more preferable target for anti-Aβ drugs, and several trials of BACE1 inhibitors (BSIs) have been conducted (Barão et al., 2016; Vassar et al., 2014). However, *in vivo* studies, based on BACE1 null mice or BSI treatment have revealed that BACE1 plays roles in several essential neural phenomena, including myelination, ion channel activities, neuronal migration, neuronal excitation, astrogenesis, and muscle spindle activity, among others (Cheret et al., 2013; Hu et al., 2016). Thus, the safety profiles of BSIs should be seriously considered and closely monitored (Barão et al., 2016; Yan, 2016). Furthermore, positron emission tomography (PET) imaging of amyloid and cerebrospinal fluid (CSF) biomarkers, such as the Aβ42/40 ratio, has shown that amyloid burden in human brains begins about 2 decades before the presentation of overt clinical symptoms of AD (Jack et al., 2013). To prevent AD development, anti-Aβ therapy that is safe and applicable for the long preclinical phase of AD without extensive amyloid burden is desirable. To realize this ideal, we set up a compound screen for a drug-repositioning approach, which has great advantages for research and development costs and time due to enormous post-marketing safety information.

Here, we established a screening platform to explore anti-Aβ compound and combined hit compounds to maximize their anti-Aβ effects. Additionally, we conducted an *in vitro* evaluation study by using iPSC-derived neurons from 13 individuals, including familial and sporadic AD patients, and confirmed that the combination of anti-Aβ compounds could reduce Aβ efficiently in all participants beyond the differences in drug responsiveness among multiple individuals. The models and process of this study should contribute to overcoming possible drawbacks of drug discovery and development by a standard platform using human iPSCs.

RESULTS

Robustly Differentiated Cortical Neurons Ensure Fine Aβ Phenotypes

Technically, the lack of consistent differentiation efficacy with a high purity of iPSCs to neurons has been an issue for precise modeling of the pathological condition and subsequent drug screening (Inoue et al., 2014). To overcome this issue, we utilized direct conversion technology to differentiate human iPSCs into cortical neurons (Davis et al., 1987; Vierbuchen et al., 2010) (Figure 1A). Direct neural conversion using lentiviral induction of neurogenin 2 (NGN2) was reported to provide mature neurons with 75%–100% purity (MAP2 [microtubule-associated protein 2]-positive cells for lentivirally infected GFP-positive cells) (Zhang et al., 2013), but the total neuronal purity (neurons per total cells in a dish) depends on the efficiency of the lentiviral infection. To

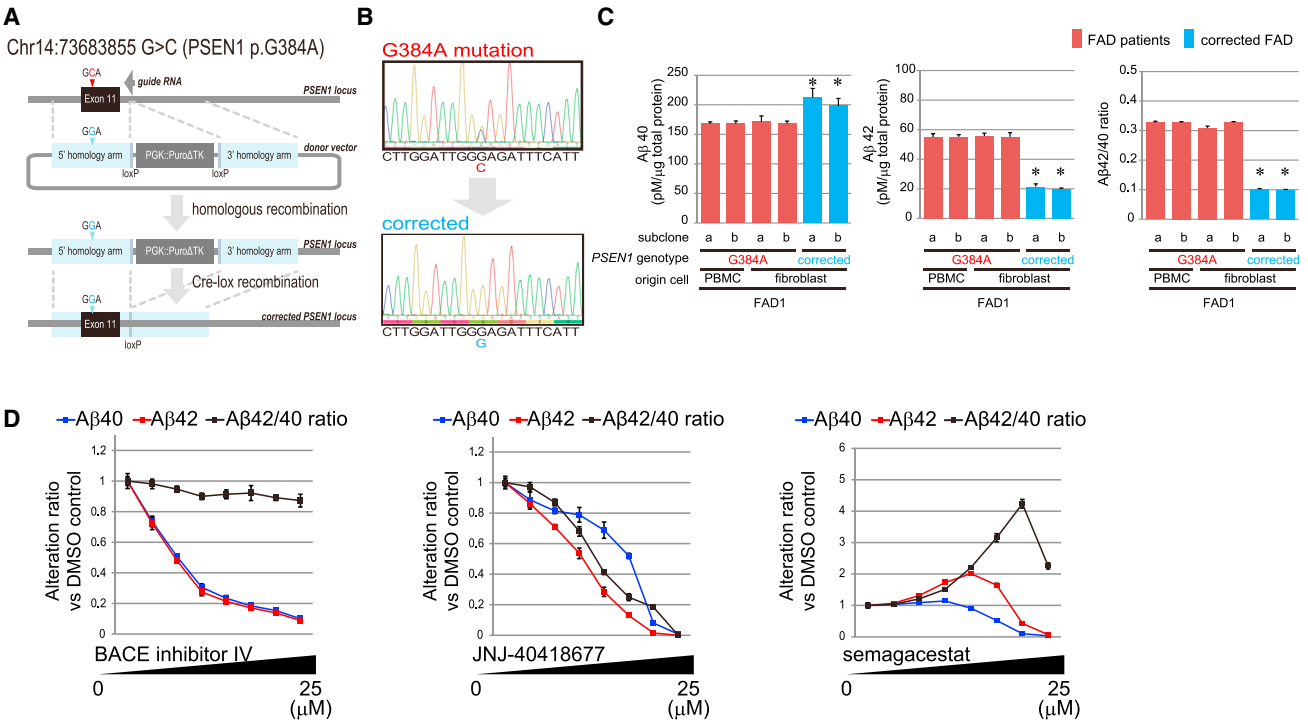

Figure 2. Alzheimer's Disease Patient Cortical Neurons Showed Aβ Phenotypes, Corrected by Genome Editing

(A) Schema of genome editing for *PSEN1* exon11, using the CRISPR-Cas9 system.

(B) Sanger-sequence data of the genome-corrected site in *PSEN1* G384A.

(C) Aβ phenotypes of iPSC-derived cortical neurons. Data indicate mean ± SD (n = 3 for each clone; *p < 0.05, Dunnett's test for multiple comparisons to FAD1 PBMC origin).

(D) ELISA quantification of Aβ species, altered by adding BSI-IV (β-secretase inhibitor), JNJ-40418677 (γ-secretase modulator), or semagacestat (γ-secretase inhibitor). Plots show the results of serial 5-fold dilutions ranging from 1.6 nM to 25 μM of the respective compounds. Data indicate mean ± SD (n = 3 for each concentration).

transduce NGN2 into all cells in a dish, we established human iPSC clones with doxycycline-inducible human NGN2 from a familial AD patient bearing a heterozygous G384A mutation of the *PSEN1* gene, which encodes presenilin-1, by using *piggyBac* transposon (Figure 1B) (Kim et al., 2016). We tested 5-day *NGN2* expression via genome-integrated *piggyBac* vector and found that the cortical neurons induced from iPSCs had more than 96% purity (Figures 1C and 1D) and expressed no remaining exogenous *NGN2* (Figure S1A) on day 8. Further, the induced cortical neurons were electrophysiologically functional (Figure S1B).

Mutations of *PSEN1* are known to increase the production of Aβ42 as a toxic Aβ species, and the Aβ42/40 ratio is an index of Aβ toxicity (Citron, 2010), compared with wild genotype (Page et al., 2008). To confirm that the system developed in this study can recapitulate the Aβ phenotypes of *PSEN1* mutation precisely, we corrected the *PSEN1* G384A mutation of FAD1 by using CRISPR-Cas9 technology (Figures 2A and 2B). Cortical neurons with a heterozygous G384A mutation in *PSEN1* produced a larger amount of Aβ42 and showed a higher Aβ42/40 ratio compared to that of neurons after genome correction (Figure 2C). Recapitulated Aβ phenotypes of FAD1 were similar to those of different iPSC clones that originated from a different type of FAD1 somatic cells (Figures 2C, S2A, and S2B). These results confirmed that our Aβ assay can provide precise phenotypes of FAD and that it offers reproducible evaluation of different iPSC clones. We also validated our assay system by applying commercially available Aβ production-modifying compounds, including β-secretase inhibitor IV (BSI-IV), JNJ-40418677 (second-generation γ-secretase modulator: GSM), and semagacestat (γ-secretase inhibitor: GSI) as positive controls and confirmed the inhibitory effects of the compounds on Aβ production (Figure 2D). On the other hand, paradoxically, a low concentration of semagacestat increased Aβ42, and a low concentration of non-steroidal anti-inflammatory drugs (NSAIDs), which are first-generation GSMs, failed to improve Aβ levels (Figure S2C), which is consistent with previous reports (Liu et al., 2014; Mertens et al., 2013; Yahata et al., 2011). From these results, we confirmed the establishment of a robust and reproducible screening system to assess changes in Aβ production in response to test compounds.

Screening for Anti-Aβ Compounds Using a Pharmaceutical Compound Library

We screened a compound library that consists of 2 μM each of 1,258 pharmaceutical compounds and ran tests to find anti-Aβ compounds as a first-step screening (Figure 3A). We defined 0.1% DMSO as a baseline control, 2 μM BSI-IV as a positive

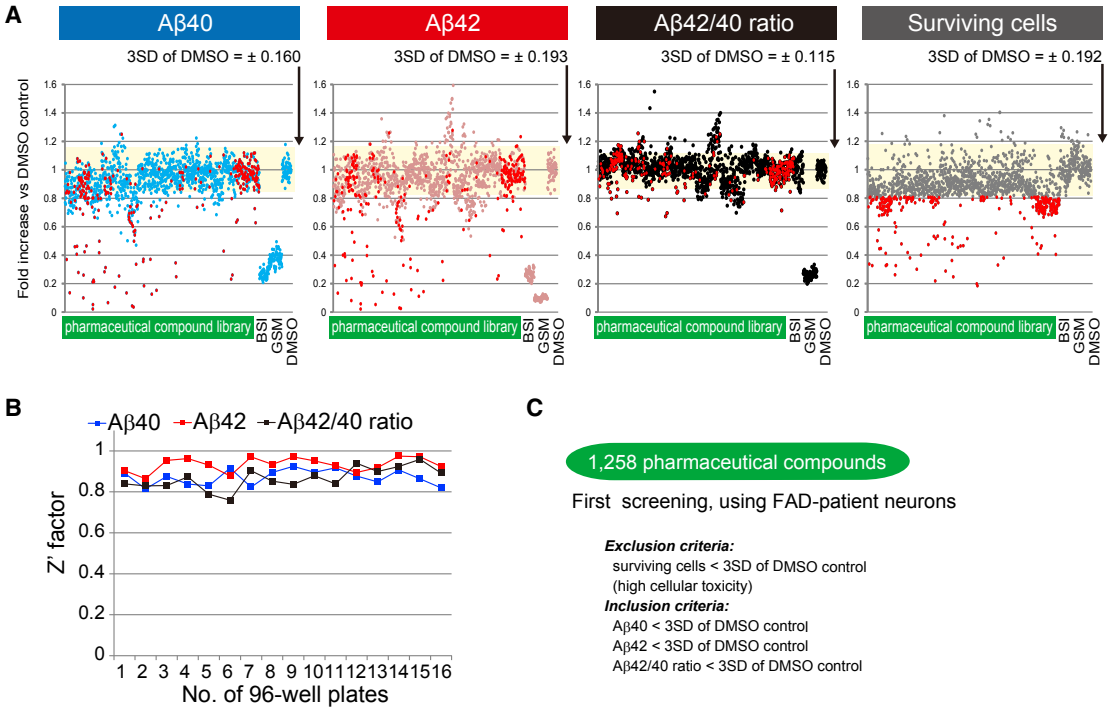

Figure 3. First-Step Screening of a Pharmaceutical Compound Library

(A) Scatterplot graphs of the first-step screening. Fold changes compared with DMSO control were plotted according to each analyte, including Aβ40 (blue), Aβ42 (red), the Aβ42/40 ratio (black), and surviving cells (gray), by adding hit compounds or positive control compounds. The 3SD variance of DMSO control groups is indicated by the yellow band. Compounds causing less survival than 3SD of DMSO control are indicated by overlapping deep red dots. BSI, β-secretase inhibitor; GSM, γ-secretase modulator.

(B) Points represent the Z' factor of each 96-well plate in the first-step screening.

(C) Criteria of the first-step screening.

control for alteration in Aβ40 production, and 2 μM JNJ-40418677 as a positive control for alteration in Aβ42 production and the Aβ42/40 ratio alteration in each assay using a 96-well-plate. Through all screening sets, Z' factor, an indicator of screening feasibility and reproducibility, was suitably high—more than 0.8—in each analyte (Figure 3B). The coefficient of variation (%CV) of DMSO control in each assay plate was below 5% (Figure S3A). From these results, we could confirm that this screening system successfully assessed dynamic Aβ responses and had low variability among the assay sets. We set the inclusion criteria of the first-step screening at "more than threefold of standard deviation values (3SD) of DMSO control in each analyte" to collect a wide range of potential anti-Aβ compounds (below the yellow field in the Figure 3A graph of Aβ40, Aβ42, and the Aβ42/40 ratio). To leave out toxic compounds that could ostensibly lead to Aβ reduction from a decreased number of neurons, we excluded compounds that caused cell survival to be less than 3SD of DMSO control (red dots in Figure 3A). According to the inclusion and exclusion criteria of the first-step screening, we collected 129 compounds (Figure 3C; Data S1). In the next step, to set stringent hit criteria, we tested the 129 compounds on both FAD1 iPSC-derived neurons and another iPSC-derived neurons, originating from peripheral blood mononuclear cells (PBMCs) of FAD1 (named "PBMC origin"). To confirm the screening reproducibility, we measured again the anti-Aβ effects of 129 compounds at 1 μM each as the second-step screening by plotting the fold-change in Aβ42, a toxic Aβ with a higher propensity to form insoluble Aβ in amyloid plaques of AD brain (Walsh et al., 2002). We observed a high correlation between FAD1 fibroblast-origin and FAD1 PBMC-origin neurons (Figure S3B). As a result, we could confirm the reproducibility of the developed screening system between different iPSC clones, and finally selected 27 screen hits that passed the inclusion criteria of Aβ42.

Chemical Structure Clustering Identified Six Lead Compounds

The anti-Aβ effects of the 27 screen hits were not as strong as those of known BSIs, GSMs, or GSIs. To select synergistic combinations with maximal anti-Aβ effects, we attempted to classify and prioritize hit compounds based on fingerprinting of the compound chemical structure (Figures 4A and S4A). The fingerprinting technique is widely used, and it successfully detects structurally diverse active compounds of various similarity levels (Gardiner et al., 2011; Vogt et al., 2010). We converted the chemical structures of 129 compounds after the first-step screening along with those of known BSIs, known GSMs, and known GSIs (Data S2) into the fingerprinting format by using the

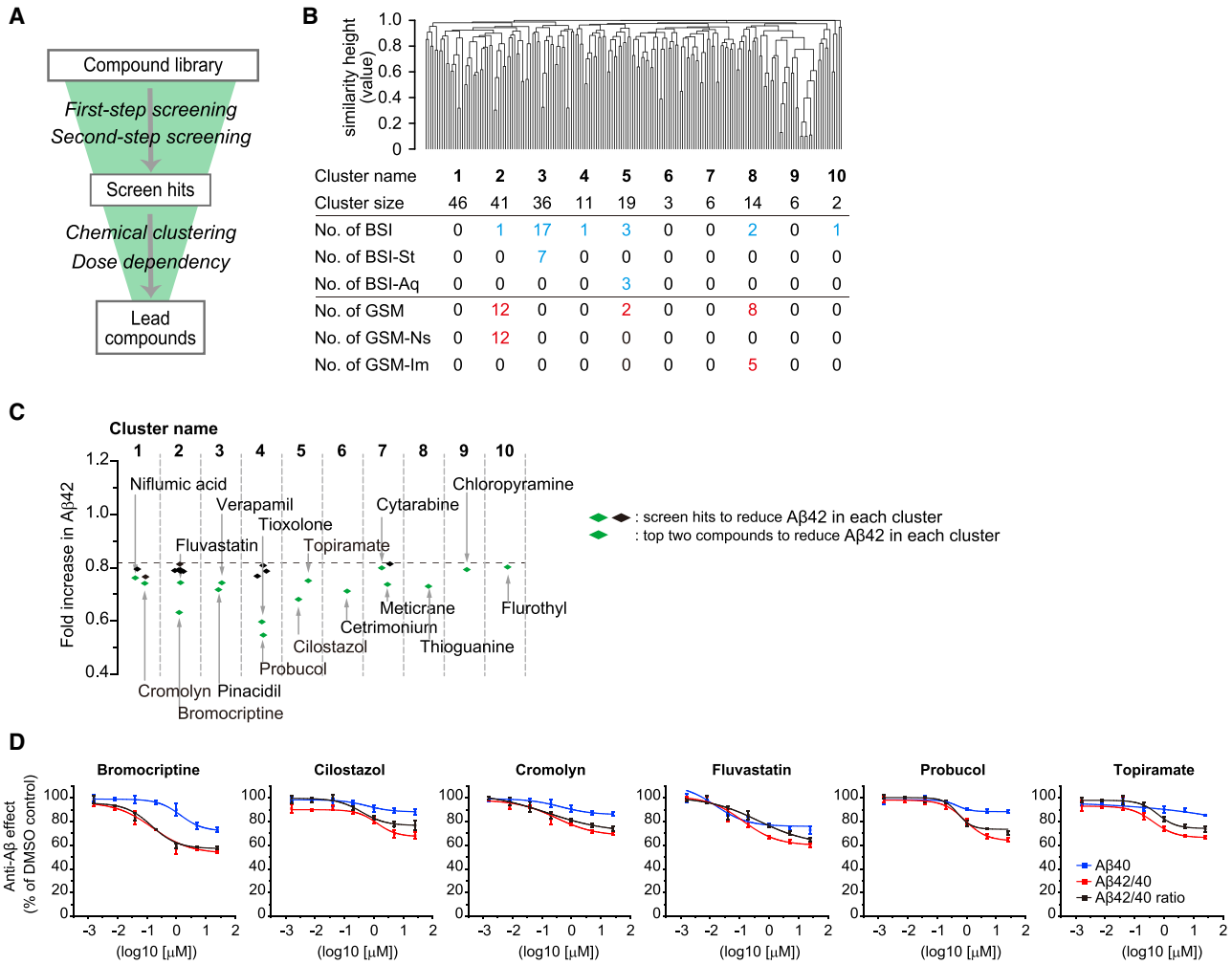

Cluster name	1	2	3	4	5	6	7	8	9	10
Cluster size	46	41	36	11	19	3	6	14	6	2
No. of BSI	0	1	17	1	3	0	0	2	0	1
No. of BSI-St	0	0	7	0	0	0	0	0	0	0
No. of BSI-Aq	0	0	0	0	3	0	0	0	0	0
No. of GSM	0	12	0	0	2	0	0	8	0	0
No. of GSM-Ns	0	12	0	0	0	0	0	0	0	0
No. of GSM-Im	0	0	0	0	0	0	0	5	0	0

Figure 4. Chemical Structure Clustering Identified Six Lead Compounds

(A) Schema of the screening steps.

(B) Chemical-structure clustering classified 129 compounds, filtered by first-step screening, and 54 known Aβ modifiers into 10 clusters, based on ECFP4 fingerprint similarity. The small table shows the number of compounds in each cluster, or known-Aβ modifiers in each cluster, including BSIs or GSMs. BSI-St, statin-derived BSI; BSI-Aq, aminoquinazoline-based BSI; GSM-Ns, NSAIDS-based GSMs; GSM-Im, GSM with imidazole structure.

(C) The Aβ42 alteration ratio (versus DMSO control) of 27 screen hits is shown in the scatterplot graph according to each cluster. Each compound name of the top two compounds to reduce Aβ42 in each cluster is labeled.

(D) The selected six anti-Aβ compounds decreased Aβ production in a dose-dependent manner. Data indicate mean ± SD (n = 3 for each clone).

Extended Connectivity Fingerprints method ([ECFP] version 4; ECFP4), which is suitable for computer processing (Rogers and Hahn, 2010). We divided various fingerprints into ten clusters by calculating a measure of molecular similarity using the Tanimoto coefficient (Tc), which is the gold standard in the chemoinformatics field (Willett et al., 1998). Tc is a numerical measure of similarity ranging from zero (no fingerprint overlap) to one (fingerprint identity). A high Tc among different compounds has generally shown similar pharmacological activities in several studies (Jasial et al., 2016). Fingerprints of the compounds were examined for any similarity of structural formulas through clustering analysis based on a distance matrix (Figure 4B). After clustering, we could separate the BSIs with similar structures into one group; for instance, statin-derived BSIs (BSI-Sts) into cluster 3 or aminoquinazoline-based BSIs (BSI-Aqs) into cluster 5. We could also separate the GSMs with similar structures into one group; for instance, NSAID-based GSMs (GSM-Ns) into cluster 2 or GSMs with imidazole structure (GSM-Ims) into cluster 8. For these investigations, we successfully carried out non-biased chemical structure clustering and classified the compounds and known Aβ-processing modifiers into ten groups (Figure 4C). To select potent anti-Aβ compounds from each group, we selected the top two compounds from each cluster and investigated whether dose-dependent reactivity to these compounds could be seen (Figure 4C). We found 11 compounds with dose-dependency Aβ42 reduction and excluded 5 compounds because they caused massive cell death at higher concentrations of 5–25 μM (Figure S4B). Finally, six compounds (bromocriptine, cilostazol,

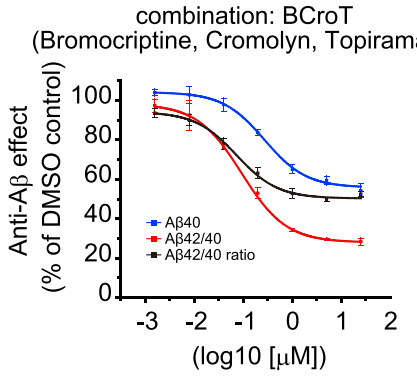

Figure 5. Combination of Anti-Aβ Compounds Improved Alzheimer's Disease Phenotypes

Combination of anti-Aβ compounds (BCroT) decreased Aβ production in a dose-dependent manner. Data indicate mean ± SD (n = 3 for each clone). BCroT, combination of bromocriptine, cromolyn, and topiramate.

cromolyn, fluvastatin, probucol, and topiramate) that showed dose-dependent Aβ42 reduction and high maximum effect (Emax) (more than −0.25) were chosen as lead compounds (Figure 4D). All but bromocriptine have been reported to show *in vivo* anti-Aβ effects (Table S1). However, we identified bromocriptine as having the most potent anti-Aβ effect. We conducted additional experiments on bromocriptine to investigate the candidate structure that modifies Aβ metabolism. First, we evaluated various dopamine receptor stimulants and determined that only bromocriptine, a specific agonist to dopamine receptor D2 subtype (DRD2), could alter Aβ metabolism (Figure S4C). Next, we compared the effect on Aβ metabolism between DRD2 agonists that include and those that exclude the ergoline structure. Potent DRD2 agonists without the ergoline structure, including talipexole and pramipexole, did not alter Aβ metabolism (Figure S4D). On the other hand, DRD2 agonists with the ergoline structure, including bromocriptine, pergolide, and cabergoline, altered Aβ metabolism (Figure S4D). These results revealed that the ergoline structure, and not the DRD2-agonistic effect, is important for altering the Aβ metabolism of human neurons. Additionally, we confirmed that compounds with the ergoline structure, which have a more than 80% structure similarity to bromocriptine, alter Aβ metabolism in a dose-dependent manner (Figure S4E), and we found that the ergot-alkaloid structure, which contains a tripeptide structure, acts to reduce Aβ production. From these results, our screening system of patient iPSC-derived neurons could select appropriate hits on the basis of the anti-Aβ effect from a compound library.

A Combination of Three Compounds Can Decrease Toxic Aβ

To maximize the anti-Aβ effects, we combined the six lead compounds, all of which have different structures. We analyzed every possible combination of the six compounds (Figure S5) and identified a combination of three (bromocriptine, cromolyn, topiramate [BCroT]) as the most potent anti-Aβ combinations. These three compounds belonged to different clusters (Figure 4C). Examining the dose-dependent curves of BCroT for Aβ42, we found a half maximal effective concentration (EC_{50}) value of 1.0 μM, and Emax values exceeding 70% reduction were seen (Figure 5).

Surveying Pharmacological Responses of Multiple Individuals

Up to this point, the analysis was conducted using FAD neurons with the *PSEN1* G384A mutation (clone name FAD1). To demonstrate the effect of BCroT on expanded populations, we conducted *in vitro* studies by using iPSCs from multiple individuals. We carried out the evaluation by using four additional iPSCs with AD-causative mutations in *PSEN1* or *APP* (clone name "FAD"), four sporadic AD iPSCs (clone name "SAD"), and six control iPSCs (clone name "HC" or "Corrected") (Figure 6A). The established human iPSCs showed pluripotency markers (Figure S6A) and could be converted into cortical neurons with more than 96% purity (Figures S6B–S6D). The combination of anti-Aβ compounds in the cocktail successfully showed more than 30% reduction in both Aβ40 and Aβ42 levels in all clones (Figures 6B) and also a reduced high Aβ42/40 ratio of PSEN1-mutated FADs (Figure 6B). From these results, we could highlight the combination of existing drugs as a new potential anti-Aβ cocktail for AD.

DISCUSSION

In this study, we have developed a robust and rapid method of neural induction from human iPSCs. Using these cells, we screened pharmaceutical compounds and found that BCroT attenuated Aβ phenotypes efficiently. Finally, we confirmed the efficacy of the anti-Aβ cocktail using iPSC-derived neurons from multiple AD patients. Accordingly, we propose a platform of drug discovery and development using human iPSCs and compound screening.

Since AD prevention requires early intervention and long-term usable drugs with validated safety, we screened pharmaceutical compounds to identify anti-Aβ compounds, although hit compounds were predicted to show a relatively weak effect on Aβ metabolism, compared with direct inhibitors of β- or γ-secretase. Therefore, we combined screen hits having different action sites to gain synergistic effects. For this purpose, we conducted chemical clustering of the hit structures, based on the hypothesis that compounds with different chemical structures target different molecules. We selected 6 compounds and identified BCroT as having synergistic anti-Aβ effects. These results suggested that the chemical clustering approach is useful for determining synergistic combinations of compounds. Additionally, we found that the stimulation of dopamine receptors, which are targets of bromocriptine, did not alter Aβ metabolism, and we identified the ergoline ring as a key structure for reducing Aβ production. These results indicated that bromocriptine may reduce the Aβ level by modifying the targets of ergot alkaloids (Wallwey and Li, 2011).

The anti-Aβ cocktail of BCroT possessed a potent inhibitory effect on Aβ production in cortical neurons from AD patients with mutant *PSEN1* and effectively diminished toxic Aβ to less than 40%, which is the same level achieved with general BSI or GSM treatment. At the same time, BCroT showed a modest

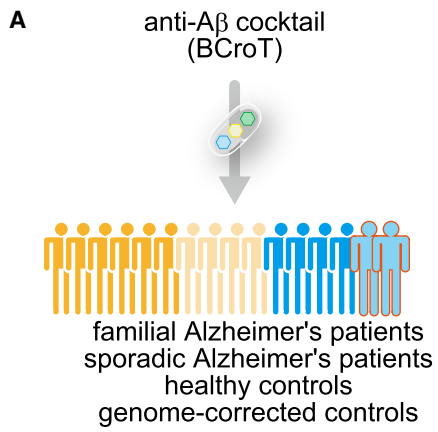

iPSC clone	karyotype	onset (age)	sampling (age)	genotype		
				APP	*PSEN1*	*APOE*
FAD1	46 XX	38	41	wild/wild	G384A/wild	2, 3
FAD2	46 XY	47	47	wild/wild	H163R/wild	3, 3
FAD3	46 XY	N.A	53	wild/wild	M146L/wild	3, 3
FAD4	46 XY	49	44	wild/wild	A246E/wild	3, 3
FAD5	46 XY	45	57	V717L/wild	wild/wild	3, 3
FAD1 PBMC-origin	46 XX	38	42	wild/wild	G384A/wild	2, 3
SAD1	46 XY	55	60	wild/wild	wild/wild	3, 3
SAD2	46 XY	72	78	wild/wild	wild/wild	4, 4
SAD3	46 XY	72	79	wild/wild	wild/wild	3, 4
SAD4	46 XX	50	60	wild/wild	wild/wild	3, 4
HC1	46 XX	-	36	wild/wild	wild/wild	3, 3
HC2	46 XX	-	51	wild/wild	wild/wild	2, 3
HC3	46 XX	-	69	wild/wild	wild/wild	3, 3
HC4	46 XY	-	47	wild/wild	wild/wild	3, 3
Corrected 1, originated from FAD1	46 XX	38	41	wild/wild	wild/wild	2, 3
Corrected 2, originated from FAD1	46 XX	38	41	wild/wild	wild/wild	2, 3

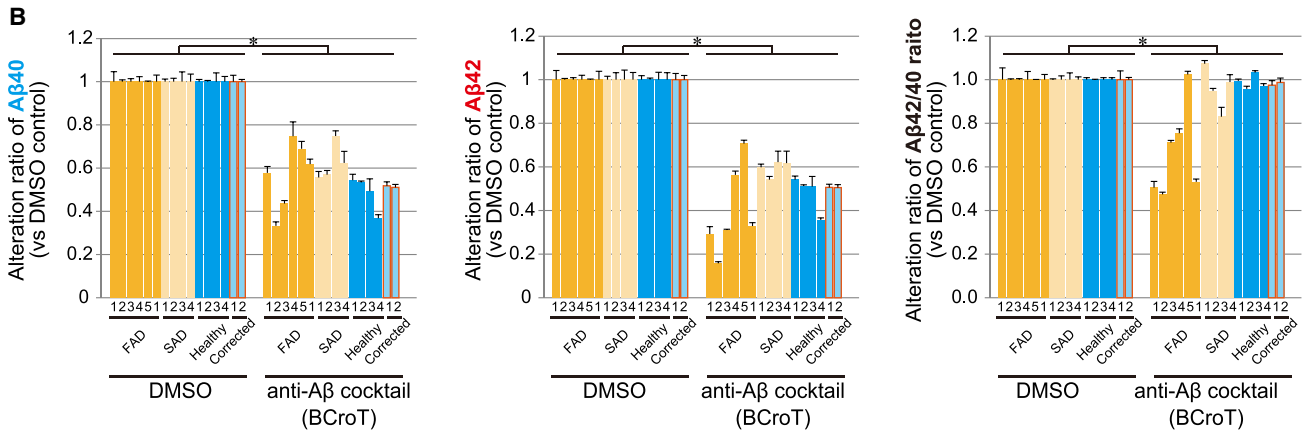

Figure 6. Anti-Aβ Cocktail of BCroT Decreased Toxic Aβ in Cortical Neurons from a Variety of Individuals

(A) Left: schema of the *in vitro* trials of BCroT in human iPSC-derived neurons from multiple individuals. BCroT, combination of bromocriptine, cromolyn, and topiramate. Right: patient information and generated iPSC characters. PBMC, peripheral blood mononuclear cell; FAD, familial Alzheimer's disease; SAD, sporadic Alzheimer's disease; HC, healthy control.

(B) BCroT suppressed the production of Aβ40 (left), Aβ42 (middle), and the Aβ42/40 ratio (right), even in FAD and SAD neurons other than FAD1 neurons. Data indicate mean ± SD (n = 3 for each clone) (n = 16 clones for each group; *p < 0.05).

effect on cortical neurons from sporadic AD and healthy control iPSCs, with a 20%–30% reduction of toxic Aβ levels. A recent Icelandic genome-cohort study revealed that the *APP* A673T mutation located adjacent to the β-cleavage site showed a 20%–30% reduction in Aβ production and was resistant to the onset of AD (Jonsson et al., 2012), suggesting that the modest effect of the anti-Aβ cocktail, BCroT, could be sufficient to prevent AD development if given to preclinical-AD patients. Furthermore, the difference of drug responsiveness between familial AD with *PSEN1* mutation and sporadic AD indicates that the individual genetic background contributes to the responsiveness, and thus, in the future, personalized compound screening would be useful for identifying more effective compounds.

In this study, we used pure cortical neurons differentiated from human iPSCs for the compound screening. This approach ignores interactions of these neurons with vascular cells, glial cells, and the blood-brain barrier. For this reason, we were unable to translate the anti-Aβ effects directly to the clinical study. With this in mind, mixed cultures of multiple cell types would be valuable for mimicking the complexity of the brain. Furthermore, when applying *in vitro* results to *in vivo* efficacy, the brain bioavailability of orally administered compounds should be considered. Bromocrpitine and topiramate are known to be efficiently delivered into brain, and cromolyn can alter brain phenotypes in various animal models (Hori et al., 2015; San-Martín-Clark et al., 1995). However, pharmacokinetic data of the anti-Aβ cocktail BCroT are not available, and it is difficult to recapitulate the absorption, degradation, and clearance of compounds through the whole body with an *in vitro* model. In future studies, the administration of the anti-Aβ cocktail BCroT to mice with AD might provide direct *in vivo* evidence for feasible clinical trials.

EXPERIMENTAL PROCEDURES

Ethical Approval

This study was approved by the Ethics Committee of the Graduate School and Faculty of Medicine, Kyoto University, and the Kyoto University Hospital (approval numbers R0091 and G259).

Generation of iN-iPSCs

To establish a robust and rapid differentiation method, we utilized direct conversion technology. Human NGN2 cDNA, under tetracycline-inducible promoter (tetO), was transfected into iPSCs by a *piggyBac* transposon system (Kim et al., 2016) and Lipofectamine LTX (Thermo Fisher Scientific, Waltham, MA). We mainly used the vector containing tetO::NGN2 (Figure 1A) and, additionally, used another vector containing TetO::NGN2-IRES-mCherry only to evaluate the time-dependent decrease of the transgenes (Figure S1B). After antibiotic selection of G418 disulfate (Nacalai-Tesque, Kyoto, Japan), we picked out colonies and selected subclones that could efficiently differentiate into neurons by inducing the temporal expression of NGN2, with MAP2/DAPI purity > 96%.

First-Step Screening

On day 0, iN-iPSCs were dissociated with TrypLE Express (GIBCO, Thermo Fisher Scientific) and disseminated on a mixed coating of poly-L-lysine (final 0.0002% v/w, Sigma Aldrich, Japan), Corning Synthemax II-SC (final 20 μg/mL, Corning, NY), and Matrigel (final 2% v/v, Corning). Disseminated iPSCs were cultured in Neurobasal Medium (GIBCO, Thermo Fisher Scientific) supplemented with 0.5% B27 without vitamin A (GIBCO, Thermo Fisher Scientific), 1× Glutamax (GIBCO, Thermo Fisher Scientific), 2 μg/mL doxycycline hydrochloride (Wako Pure Chemicals Industries, Japan), and 5 μM Y-27632 (Nacalai-Tesque) from day 0 to day 5. On day 5, differentiated neural cells were disseminated into 96-well plates by passive humidity control (Nunc Edge plates, Thermo Fisher Scientific), which can eliminate the evaporation of culture medium and minimize well-to-well variability. Disseminated neural cells were cultured in Neurobasal Medium supplemented with 0.5% B27 without vitamin A and 1× Glutamax from day 5 to day 8. On day 8, all culture media were replaced with 120 μL fresh medium, containing each of the 2 μM of each compound in final 0.1% DMSO carrier or only 0.1% DMSO. Neurons or culture media were subjected to analysis 48 hr later.

Pharmaceutical Compound Library

We used the Microsource International Drug and Microsource US Drug library, which includes a total of 1,258 pharmaceutical compounds that have reached clinical trial stages in the United States. Each compound has been assigned United States Adopted Names (USAN) or United States Pharmacopeiah (USP) status and is included in the USP Dictionary. Each 96-well plate contained 80 compounds per plate, four positive controls for Aβ40 (2 μM BSI-IV), four positive controls for Aβ42 and the Aβ42/40 ratio (2 μM JNJ-40418677), and eight negative controls (0.1% DMSO carrier). The raw data of each compound or positive control were normalized to calculate the alteration ratio by using the average data of the eight DMSO controls in each plate (the alteration ratio = raw data of each compound/averaged data of eight DMSO controls in each plate).

Structure-Based Clustering of Chemical Compounds

We prepared a list of additional chemical compounds, including (1) the first-step screening active compounds (n = 129) and (2) previously reported β- or γ-secretase modifier compounds (n = 55). We classified the total 184 compounds into 10 hierarchical clusters based on similarity (entrusted to Kyoto Constella Technologies, Japan). The similarity (Tc: Tanimoto coefficient) among compounds is defined using the ECFP4 fingerprint method (Rogers and Hahn, 2010), as calculated by jCompoundMapper (Hinselmann et al., 2011). The distance was defined as "Distance = 1 − Tc." We decided on a comprehensive distance matrix among all 184 compounds and finally classified compounds into 10 similar hierarchical clusters by the furthest neighbor method, using the statistical software tool "R."

Statistical Analysis

All data are indicated as mean ± SD. For comparisons of the mean between two groups, statistical analysis was performed using a two-tailed Student's t test. For comparisons of the mean among more than three groups, statistical analysis was performed using a one-way ANOVA, followed by a post hoc test using Dunnett's test. All analyses were performed by using JMP 9 software (SAS Institute, Cary, NC). p values < 0.05 were considered significant.

SUPPLEMENTAL INFORMATION

Supplemental Information includes Supplemental Experimental Procedures, six figures, one table, and two data files and can be found with this article online at https://doi.org/10.1016/j.celrep.2017.10.109.

AUTHOR CONTRIBUTIONS

H.I. conceived the project. T.K., N.I., and H.I. designed the experiment. T.K., K.I., M.F., K.T., M.M., and H.I. performed the experiments and analyzed the data. K.I. performed neurophysiological procedures. A.O. provided compound libraries. K.W. and M.N. provided the materials and supervised the vector constructions and iPSC cultivation method. S.K., T. Asada, T. Arai, Y.I., and R.K. provided patient samples and information. T.K., N.I., and H.I. wrote the manuscript.

ACKNOWLEDGMENTS

We would like to express our sincere gratitude to all our coworkers and collaborators; to Takako Enami and Ran Shibukawa for technical assistance; to Peter Karagiannis for critical reading and editing of the manuscript; and to Noriko Endo and Ruri Taniguchi for their valuable administrative support. This research was funded in part by the Research Project for Practical Applications of Regenerative Medicine from AMED (to H.I.); a grant from the Core Center for iPSC Research of Research Center Network for Realization of Regenerative Medicine from AMED (to H.I.); and a JSPS KAKENHI Grant-in-Aid for Young Scientists (B) 17K16121 (to T.K.). The experimental protocols dealing with human or animal subjects were approved by the institutional review board of each institute.

Received: February 24, 2016
Revised: September 17, 2017
Accepted: October 26, 2017
Published: November 21, 2017

REFERENCES

Barão, S., Moechars, D., Lichtenthaler, S.F., and De Strooper, B. (2016). BACE1 physiological functions may limit its use as therapeutic target for Alzheimer's disease. Trends Neurosci. *39*, 158–169.

Cheret, C., Willem, M., Fricker, F.R., Wende, H., Wulf-Goldenberg, A., Tahirovic, S., Nave, K.-A., Saftig, P., Haass, C., Garratt, A.N., et al. (2013). Bace1 and Neuregulin-1 cooperate to control formation and maintenance of muscle spindles. EMBO J. *32*, 2015–2028.

Citron, M. (2010). Alzheimer's disease: strategies for disease modification. Nat. Rev. Drug Discov. *9*, 387–398.

Davis, R.L., Weintraub, H., and Lassar, A.B. (1987). Expression of a single transfected cDNA converts fibroblasts to myoblasts. Cell *51*, 987–1000.

De Strooper, B. (2014). Lessons from a failed γ-secretase Alzheimer trial. Cell *159*, 721–726.

Filser, S., Ovsepian, S.V., Masana, M., Blazquez-Llorca, L., Brandt Elvang, A., Volbracht, C., Müller, M.B., Jung, C.K.E., and Herms, J. (2015). Pharmacological inhibition of BACE1 impairs synaptic plasticity and cognitive functions. Biol. Psychiatry *77*, 729–739.

Gardiner, E.J., Holliday, J.D., O'Dowd, C., and Willett, P. (2011). Effectiveness of 2D fingerprints for scaffold hopping. Future Med. Chem. *3*, 405–414.

Hardy, J., and Selkoe, D.J. (2002). The amyloid hypothesis of Alzheimer's disease: progress and problems on the road to therapeutics. Science *297*, 353–356.

Hinselmann, G., Rosenbaum, L., Jahn, A., Fechner, N., and Zell, A. (2011). jCompoundMapper: An open source Java library and command-line tool for chemical fingerprints. J. Cheminform. *3*, 3.

Hori, Y., Takeda, S., Cho, H., Wegmann, S., Shoup, T.M., Takahashi, K., Irimia, D., Elmaleh, D.R., Hyman, B.T., and Hudry, E. (2015). A Food and Drug Administration-approved asthma therapeutic agent impacts amyloid β in the brain in a transgenic model of Alzheimer disease. J. Biol. Chem. *290*, 1966–1978.

Hu, X., Fan, Q., Hou, H., and Yan, R. (2016). Neurological dysfunctions associated with altered BACE1-dependent Neuregulin-1 signaling. J. Neurochem. *136*, 234–249.

Inoue, H., Nagata, N., Kurokawa, H., and Yamanaka, S. (2014). iPS cells: a game changer for future medicine. EMBO J. *33*, 409–417.

Jack, C.R., Jr., Knopman, D.S., Jagust, W.J., Petersen, R.C., Weiner, M.W., Aisen, P.S., Shaw, L.M., Vemuri, P., Wiste, H.J., Weigand, S.D., et al. (2013). Tracking pathophysiological processes in Alzheimer's disease: an updated hypothetical model of dynamic biomarkers. Lancet Neurol. *12*, 207–216.

Jasial, S., Hu, Y., Vogt, M., and Bajorath, J. (2016). Activity-relevant similarity values for fingerprints and implications for similarity searching. F1000Res *5*, 591.

Jonsson, T., Atwal, J.K., Steinberg, S., Snaedal, J., Jonsson, P.V., Bjornsson, S., Stefansson, H., Sulem, P., Gudbjartsson, D., Maloney, J., et al. (2012). A mutation in APP protects against Alzheimer's disease and age-related cognitive decline. Nature *488*, 96–99.

Kim, S.I., Oceguera-Yanez, F., Sakurai, C., Nakagawa, M., Yamanaka, S., and Woltjen, K. (2016). Inducible transgene expression in human iPS cells using versatile all-in-one piggyBac transposons. Methods Mol. Biol. *1357*, 111–131.

Liu, Q., Waltz, S., Woodruff, G., Ouyang, J., Israel, M.A., Herrera, C., Sarsoza, F., Tanzi, R.E., Koo, E.H., Ringman, J.M., et al. (2014). Effect of potent γ-secretase modulator in human neurons derived from multiple presenilin 1-induced pluripotent stem cell mutant carriers. JAMA Neurol. *71*, 1481–1489.

Mertens, J., Stüber, K., Wunderlich, P., Ladewig, J., Kesavan, J.C.C., Vandenberghe, R., Vandenbulcke, M., van Damme, P., Walter, J., Brüstle, O., and Koch, P. (2013). APP processing in human pluripotent stem cell-derived neurons is resistant to NSAID-based γ-secretase modulation. Stem Cell Reports *1*, 491–498.

Onder, T.T., and Daley, G.Q. (2012). New lessons learned from disease modeling with induced pluripotent stem cells. Curr. Opin. Genet. Dev. *22*, 500–508.

Page, R.M., Baumann, K., Tomioka, M., Pérez-Revuelta, B.I., Fukumori, A., Jacobsen, H., Flohr, A., Luebbers, T., Ozmen, L., Steiner, H., and Haass, C. (2008). Generation of $A\beta_{38}$ and $A\beta_{42}$ is independently and differentially affected by familial Alzheimer disease-associated presenilin mutations and γ-secretase modulation. J. Biol. Chem. *283*, 677–683.

Paul, S.M., Mytelka, D.S., Dunwiddie, C.T., Persinger, C.C., Munos, B.H., Lindborg, S.R., and Schacht, A.L. (2010). How to improve R&D productivity: the pharmaceutical industry's grand challenge. Nat. Rev. Drug Discov. *9*, 203–214.

Paull, D., Sevilla, A., Zhou, H., Hahn, A.K., Kim, H., Napolitano, C., Tsankov, A., Shang, L., Krumholz, K., Jagadeesan, P., et al. (2015). Automated, high-throughput derivation, characterization and differentiation of induced pluripotent stem cells. Nat. Methods *12*, 885–892.

Powers, J.M. (1997). Diagnostic criteria for the neuropathologic assessment of Alzheimer's disease. Neurobiol. Aging *18* (*4, Suppl*), S53–S54.

Rogers, D., and Hahn, M. (2010). Extended-connectivity fingerprints. J. Chem. Inf. Model. *50*, 742–754.

San-Martín-Clark, O., Cuéllar, B., De Alba, J., Leza, J.C., and Lorenzo, P. (1995). Changes induced by sodium cromoglycate in brain catecholamine turnover in morphine dependent and abstinent mice. Psychopharmacology (Berl.) *118*, 347–353.

Selkoe, D.J. (2002). Alzheimer's disease is a synaptic failure. Science *298*, 789–791.

Selkoe, D.J.American College of Physicians; American Physiological Society (2004). Alzheimer disease: mechanistic understanding predicts novel therapies. Ann. Intern. Med. *140*, 627–638.

Shi, Y., Inoue, H., Wu, J.C., and Yamanaka, S. (2016). Induced pluripotent stem cell technology: a decade of progress. Nat. Rev. Drug Discov *16*, 115–130.

Szabo, E., Rampalli, S., Risueño, R.M., Schnerch, A., Mitchell, R., Fiebig-Comyn, A., Levadoux-Martin, M., and Bhatia, M. (2010). Direct conversion of human fibroblasts to multilineage blood progenitors. Nature *468*, 521–526.

Thatava, T., Kudva, Y.C., Edukulla, R., Squillace, K., De Lamo, J.G., Khan, Y.K., Sakuma, T., Ohmine, S., Terzic, A., and Ikeda, Y. (2013). Intrapatient variations in type 1 diabetes-specific iPS cell differentiation into insulin-producing cells. Mol. Ther. *21*, 228–239.

Vassar, R., Kuhn, P.H., Haass, C., Kennedy, M.E., Rajendran, L., Wong, P.C., and Lichtenthaler, S.F. (2014). Function, therapeutic potential and cell biology of BACE proteases: current status and future prospects. J. Neurochem. *130*, 4–28.

Vierbuchen, T., Ostermeier, A., Pang, Z.P., Kokubu, Y., Südhof, T.C., and Wernig, M. (2010). Direct conversion of fibroblasts to functional neurons by defined factors. Nature *463*, 1035–1041.

Vogt, M., Stumpfe, D., Geppert, H., and Bajorath, J. (2010). Scaffold hopping using two-dimensional fingerprints: true potential, black magic, or a hopeless endeavor? Guidelines for virtual screening. J. Med. Chem. *53*, 5707–5715.

Wallwey, C., and Li, S.-M. (2011). Ergot alkaloids: structure diversity, biosynthetic gene clusters and functional proof of biosynthetic genes. Nat. Prod. Rep. *28*, 496–510.

Walsh, D.M., Klyubin, I., Fadeeva, J.V., Cullen, W.K., Anwyl, R., Wolfe, M.S., Rowan, M.J., and Selkoe, D.J. (2002). Naturally secreted oligomers of amyloid beta protein potently inhibit hippocampal long-term potentiation in vivo. Nature *416*, 535–539.

Willett, P., Barnard, J.M., and Downs, G.M. (1998). Chemical similarity searching. J. Chem. Inf. Comput. Sci. *38*, 983–996.

Yahata, N., Asai, M., Kitaoka, S., Takahashi, K., Asaka, I., Hioki, H., Kaneko, T., Maruyama, K., Saido, T.C., Nakahata, T., et al. (2011). Anti-Aβ drug screening platform using human iPS cell-derived neurons for the treatment of Alzheimer's disease. PLoS ONE *6*, e25788.

Yan, R. (2016). Stepping closer to treating Alzheimer's disease patients with BACE1 inhibitor drugs. Transl. Neurodegener. *5*, 13.

Zhang, Y., Pak, C., Han, Y., Ahlenius, H., Zhang, Z., Chanda, S., Marro, S., Patzke, C., Acuna, C., Covy, J., et al. (2013). Rapid single-step induction of functional neurons from human pluripotent stem cells. Neuron *78*, 785–798.

Cell Reports, Volume *21*

Supplemental Information

iPSC-Based Compound Screening and *In Vitro* Trials Identify a Synergistic Anti-amyloid β Combination for Alzheimer's Disease

Takayuki Kondo, Keiko Imamura, Misato Funayama, Kayoko Tsukita, Michiyo Miyake, Akira Ohta, Knut Woltjen, Masato Nakagawa, Takashi Asada, Tetsuaki Arai, Shinobu Kawakatsu, Yuishin Izumi, Ryuji Kaji, Nobuhisa Iwata, and Haruhisa Inoue

Inventory of Supplementary Information

Supplemental Figure S1 is related to **Figure 1.**

Supplemental Figure S2 is related to **Figure 2.**

Supplemental Figure S3 and **Supplemental Spread Sheet S1** are related to **Figure 3.**

Supplemental Figure S4 and **Supplemental Spread Sheet S2** are related to **Figure 4.**

Supplemental Figure S5 and **Supplemental Table S1** are related to **Figure 5.**

Supplemental Figure S6 is related to **Figure 6.**

SUPPLEMENTAL EXPERIMENTAL PROCEDURES

Derivation of somatic cells

All human tissue collection, human stem cell studies, procedures, and written consent was approved by the Ethics Committee of the Graduate School and Faculty of Medicine, Kyoto University, and the Kyoto University Hospital. Control and AD-derived human dermal fibroblasts were generated from the explants of 3-mm dermal biopsies. AG07872-fibroblasts (origin of FAD3 iPSC) and AG07671-fibroblasts (origin of FAD4 iPSC) were obtained from the Coriell Institute for Medical Research. After 1-2 weeks, fibroblast outgrowths from the explants were passaged. Human peripheral blood mononuclear cells (PBMCs) were obtained from healthy donors and FAD1, and expanded for the generation of iPS cells (iPSCs), as previously described (Okita et al., 2012).

Generation and characterization of patient iPSCs

For iPSCs generated from fibroblasts, human cDNAs for reprogramming factors were transduced in fibroblasts with episomal vectors (SOX2, KLF4, OCT4, L-MYC, LIN28, siRNA for p53) (Kondo et al., 2013). Several days after transduction, fibroblasts were harvested and replated on an SNL feeder cell layer. On the following day, the medium was changed to primate embryonic stem cell medium (ReproCell, Yokohama, Japan) supplemented with 4 ng/mL basic FGF (Wako Pure Chemicals, Tokyo, Japan). The medium was changed every other day. Thirty days after transduction, iPSC colonies were picked up. Established fibroblast-origin iPSCs were replated on an iMatrix-coated dish (Nippi, Tokyo, Japan), maintained using StemFit AK03 medium (Ajinomoto, Tokyo, Japan) (Nakagawa et al., 2014), and expanded for neural differentiation. For iPSCs from PBMCs, human cDNAs for reprogramming factors were transduced in human PBMCs with episomal vectors (SOX2, KLF4, OCT4, L-MYC, LIN28, dominant negative p53). Several days after transduction, PBMCs were harvested and replated on an iMatrix-coated dish. On the following day, the medium was changed to StemFit AK03. The medium was changed every other day. Twenty days after transduction, iPSC colonies were picked up. Established PBMC-origin iPSCs were expanded for neural differentiation.

Genetic correction of iPSCs

iPSCs were dissociated using Tryple express (Thermo Fisher Scientific, Waltham, MA). 500,000 single cells were mixed with 400 μL Opti-MEM containing Cas9, gRNA expression vector, donor

vector, and lipofectamine LTX (Thermo Fisher Scientific), and disseminated onto iMatrix-511-coated 6-well plates with StemFit medium containing 10 μM Y27632 (Nacalai-Tesque, Kyoto, Japan). After puromycin treatment, colonies were mechanically selected. To screen genomic DNA samples for integration of the corrective sequences, the target locus was amplified by PCR. Correctly targeted iPSCs (10,000 cells) were transfected with Cre expression vector, followed by selection with FIAU. Individual colonies were mechanically selected. Corrected mutation sites were analyzed by PCR and sequencing.

Karyotyping and genotyping

Karyotyping was performed at our institute or LSI Medience (Japan). Genotyping of single nucleotide mutation was performed by PCR amplification of genomic DNA and directly sequenced (3100 Genetic Analyzer; Thermo Fisher Scientific). *APOE* gene was amplified by PCR (forward primer TCCAAGGAGCTGCAGGCGGCGCA; reverse primer ACAGAATTCGCCCCGGCCTGGTACACTG). The PCR products were digested by HhaI at 37°C for 2 hr and then subjected to electrophoresis to analyze the band size.

***In vitro* three germ differentiation**

Human iPSCs were harvested by TrypLE express (Gibco, Thermo Fisher Scientific) and used for embryoid body (EB) formation. Clumps of cells were transferred to Petri dishes in DMEM/F12 (Gibco, Thermo Fisher Scientific) containing 20% knockout serum replacement (KSR; Gibco, Thermo Fisher Scientific), 2 mM L-glutamine, 0.1 M nonessential amino acids, 0.1 M 2-mercaptoethanol (Gibco, Thermo Fisher Scientific), and 0.5% penicillin and streptomycin. The medium was changed every other day. For spontaneous differentiation, 8-day-old EBs were plated onto gelatin-coated coverslips and allowed to differentiate in DMEM, supplemented with 10% fetal bovine serum for an additional 8 days.

Quantitative RT-PCR

Total RNA was extracted by RNeasy plus kit (QIAGEN, Hilden, Germany). 500 ng of total RNA was reverse-transcribed into cDNA using RevaTra Ace with random primers (Toyobo, Osaka, Japan). To analyze gene expressions, we designed specific PCR primers of human NGN2 or mCherry.

One μL of the generated cDNA was used as template for each reaction in real-time quantitative PCR analysis, using SYBR Green II (TAKARA, Kusatsu, Japan) and StepONE plus (Thermo Fisher Scientific). GAPDH was used as housekeeping control gene to normalize the target genes. To perform relative quantification, the comparative threshold (Ct) cycle method was used. The fold change in gene expression profile in each step was referred to the gene expression of iPSCs.

Electrochemiluminescence assays for Aβ

Aβ species in culture media were measured by human (6E10) Aβ 3-Plex Kit (Meso Scale Discovery, Rockville, MD) for extracellular human Aβ. For Aβ species, this assay uses 6E10 antibody to capture Aβ peptide and SULFO-TAG-labeled different C-terminus specific anti-Aβ antibodies for detection by electrochemiluminescence with Sector Imager 2400 (Meso Scale Discovery). Quantified Aβ values were adjusted using total protein grations in neurons and compared among conditions.

Selection of structurally similar compounds to bromocriptine

Using the ChEMBL database (release 23, https://www.ebi.ac.uk/chembl/), we input the molfile of the bromocriptine structure (CHEMBL ID 493) and search structurally similar compounds with the cut off line at 80% tanimoto similarity. We purchased all compounds, which are legally available in Japan and used them for the Aβ assay.

Immunocytochemistry

Cells were fixed in 4% paraformaldehyde (pH 7.4) for 30 min at room temperature and rinsed with PBS. The cells were permeabilized in PBS containing 0.2% Triton X-100 for 10 min at room temperature, followed by rinsing with PBS. Nonspecific binding was blocked with BlockingONE Histo (Nacalai tesque) for 60 min at room temperature. Cells were incubated with primary antibodies overnight at 4°C, and then labeled with appropriate fluorescent-tagged secondary antibodies. DAPI (Thermo Fisher Scientific) was used to label nuclei. Fluorescence images were acquired on high-content confocal microscope In Cell Analyzer 6000 (GE Healthcare, Chicago, IL). The following primary antibodies were used for immunocytochemistry: NANOG (1:100 dilution; Abcam, Cambridge, UK), TRA1-60 (1:400; CST, Danvers, MA), MAP2 (1:4,000; Abcam), VGLUT1 (1:1,000; Synaptic Systems, Goettingen, Germany), and CTIP2 (1:400; Abcam).

Electrophysiological recordings

Whole-cell patch-clamp recordings were performed from iPSC-derived neurons under differential interference contrast imaging. The recording micropipettes were filled with intracellular solution consisting of 140 mM KCl, 2 mM $MgCl_2$, 10 mM HEPES, and 1 mM EGTA, adjusted to pH 7.4 with NaOH. Cells were maintained at 30°C during the experiment and were continuously superfused with oxygenated Krebs-Ringer solution consisting of 125 mM NaCl, 2.5 mM KCl, 1.25 mM NaH_2PO_4, 26 mM $NaHCO_3$, 1 mM $MgCl_2$, 2 mM $CaCl_2$, and 20 mM glucose. Voltage-clamp and current-clamp recordings were made using an EPC 9 amplifier (HEKA Elektronik, Lambrecht, Germany) and data were analyzed with Patchmaster software (HEKA).

References for SUPPLEMENTAL EXPERIMENTAL PROCEDURES

Hinselmann, G., Rosenbaum, L., Jahn, A., Fechner, N., and Zell, A. (2011). jCompoundMapper: An open source Java library and command-line tool for chemical fingerprints. J. Cheminform. *3*, 3.

Kondo, T., Asai, M., Tsukita, K., Kutoku, Y., Ohsawa, Y., Sunada, Y., Imamura, K., Egawa, N., Yahata, N., Okita, K., et al. (2013). Modeling Alzheimer's disease with iPSCs reveals stress phenotypes associated with intracellular Aβ and differential drug responsiveness. Cell Stem Cell *12*, 487–496.

Nakagawa, M., Taniguchi, Y., Senda, S., Takizawa, N., Ichisaka, T., Asano, K., Morizane, A., Doi, D., Takahashi, J., Nishizawa, M., et al. (2014). A novel efficient feeder-free culture system for the derivation of human induced pluripotent stem cells. Sci. Rep. *4*, 3594.

Okita, K., Yamakawa, T., Matsumura, Y., Sato, Y., Amano, N., Watanabe, A., Goshima, N., and Yamanaka, S. (2013). An Efficient Non-viral Method to Generate Integration-Free Human iPS Cells from Cord Blood and Peripheral Blood Cells. Stem Cells. *31*, 458–466

Rogers, D., and Hahn, M. (2010). Extended-connectivity fingerprints. J.Che.Inform.Model. *50*, 742–754.

Fig. S1

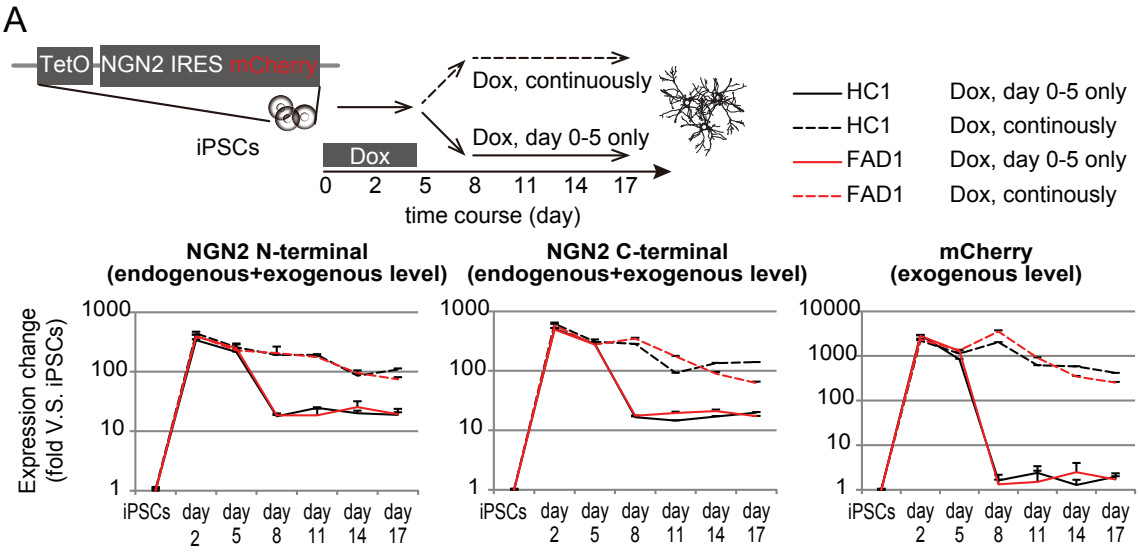
A
TetO
NGN2 IRES mCherry
iPSCs
Dox
Dox, continuously
Dox, day 0-5 only
0 2 5 8 11 14 17
time course (day)
HC1 Dox, day 0-5 only
HC1 Dox, continously
FAD1 Dox, day 0-5 only
FAD1 Dox, continously
NGN2 N-terminal (endogenous+exogenous level)
NGN2 C-terminal (endogenous+exogenous level)
mCherry (exogenous level)
Expression change (fold V.S. iPSCs)
1000
100
10
1
10000
iPSCs day 2 day 5 day 8 day 11 day 14 day 17

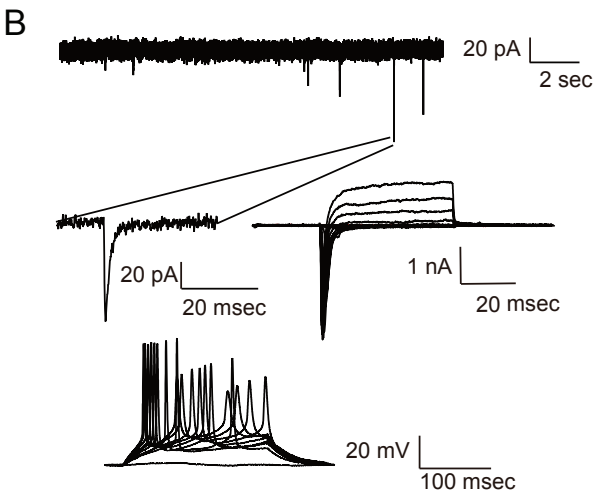
B
20 pA
2 sec
20 pA
20 msec
1 nA
20 msec
20 mV
100 msec

Supplementary Figure S1. Characterization of iPSC-derived cortical neurons, Related to Figure 1

(A) A time-dependent decrease in transgenes after depleted doxycycline (Dox). The expression level of mCherry (transgene reporter), as assessed by qPCR, had decreased rapidly by day 8. However, the expression of NGN2 retained its endogenous level even after switching off the transgene. TetO: tetracycline operator. NGN2: neurogenin 2. Dox: doxycycline. (B) Action potentials were recorded in current clamp recordings, as whole-cell voltage-clamp recordings of Na^+ (rapid inward) and K^+ (slow outward) currents. Cells were held at –60 mV, and voltage was increased stepwise from –60 mV to +30 mV at 10 mV intervals. Current-clamp recordings of spontaneous action potentials. Na^+/K^+ currents and action potentials were measured to examine whether induced neurons from iPSCs were functionally active.

Fig. S2

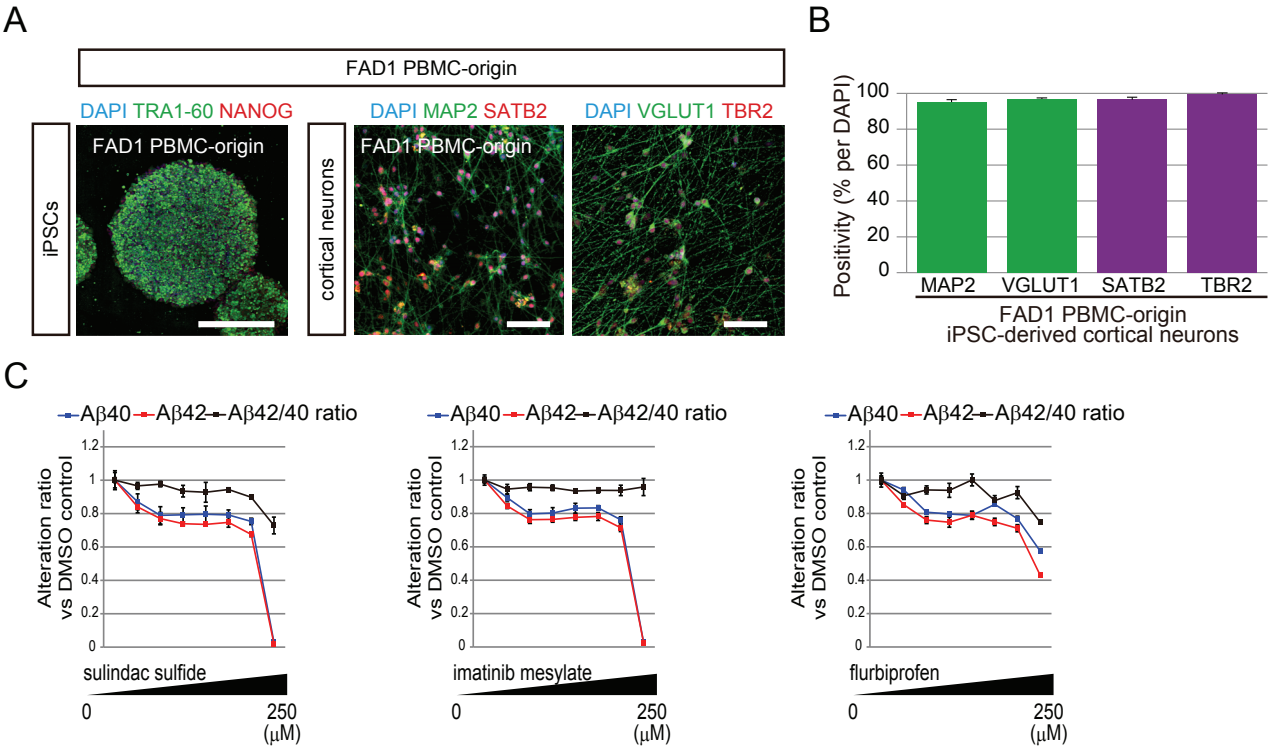
A
FAD1 PBMC-origin
DAPI TRA1-60 NANOG
DAPI MAP2 SATB2
DAPI VGLUT1 TBR2
iPSCs
FAD1 PBMC-origin
cortical neurons
FAD1 PBMC-origin
B
Positivity (% per DAPI)
100
80
60
40
20
0
MAP2
VGLUT1
SATB2
TBR2
FAD1 PBMC-origin
iPSC-derived cortical neurons
C
Aβ40 Aβ42 Aβ42/40 ratio
Alteration ratio vs DMSO control
1.2
1
0.8
0.6
0.4
0.2
0
sulindac sulfide
0
250
(μM)
Aβ40 Aβ42 Aβ42/40 ratio
Alteration ratio vs DMSO control
imatinib mesylate
0
250
(μM)
Aβ40 Aβ42 Aβ42/40 ratio
Alteration ratio vs DMSO control
flurbiprofen
0
250
(μM)

Supplementary Figure S2. First-generation GSM, did not improve Aβ phenotypes of Alzheimer's disease cortical neurons, Related to Figure 2

(A) Characterization of iPSCs and differentiated cortical neurons, originated from FAD1-PBMCs. Day 8 neurons expressed excitatory cortical neuron markers; left: MAP2 (green) and SATB2 (red) and right: VGLUT1 (green) and TBR2 (red). PBMC: peripheral blood mononuclear cells. (B) Purity of day 8 neurons. Data represent mean ± SD (n = 3 for each clone) (C) ELISA quantification of Aβ species, altered by adding known GSM, including sulindac sulfide, imatinib mesylate, and flurbiprofen. Plots show the results of serial 5-fold dilutions ranging from 1.6 nM to 25 μM of the respective compounds. Data represent mean ± SD (n = 3 for each concentration).

Fig. S3

A

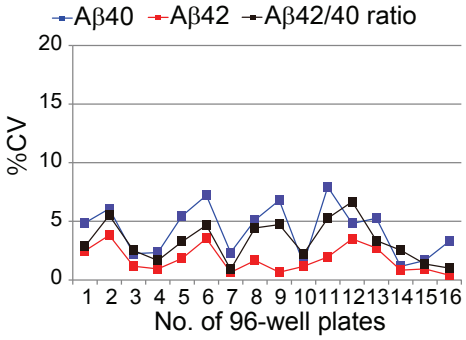
Aβ40
Aβ42
Aβ42/40 ratio
%CV
20
15
10
5
0
1 2 3 4 5 6 7 8 9 10 11 12 13 14 15 16
No. of 96-well plates

B

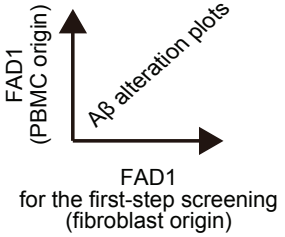
FAD1
(PBMC origin)
Aβ alteration plots
FAD1
for the first-step screening
(fibroblast origin)

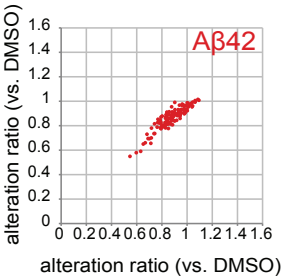
Aβ42
alteration ratio (vs. DMSO)
1.6
1.4
1.2
1
0.8
0.6
0.4
0.2
0
0 0.2 0.4 0.6 0.8 1 1.2 1.4 1.6
alteration ratio (vs. DMSO)

Supplementary Figure S3. Developed Aβ screening system was confirmed to be robust and reproducible, Related to Figure 3

(A) Each point represents the coefficient of variation (%CV) of each 96-well plate in the first-step screening, calculated by the quantified data of 8 DMSO-control wells per plate. (B) Pairwise correlation comparison of Aβ species alteration by adding 129 compounds from the first-step screening. Pearson correlation scatter plots of Aβ species alteration in PBMC-origin FAD1 neurons (Y-axis) and fibroblast-origin FAD1 neurons (X-axis). Pearson's $R^2 = 0.98$.

Fig. S4

A

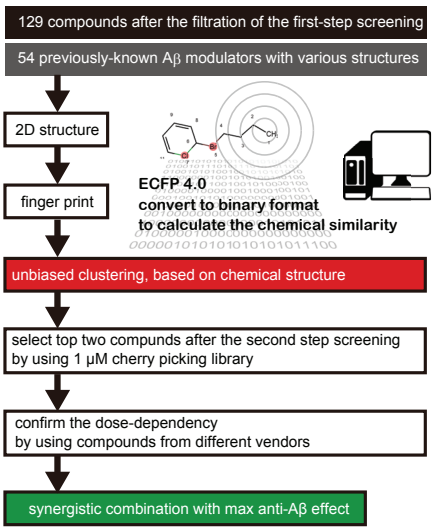

B

Screening steps	No.	rate (%)
Screened compounds	1258	
Screen hits *1	27	2.14
Dose-dependency *2	11	0.87
Toxic hits *3	5	
Lead compounds	6	0.48

C

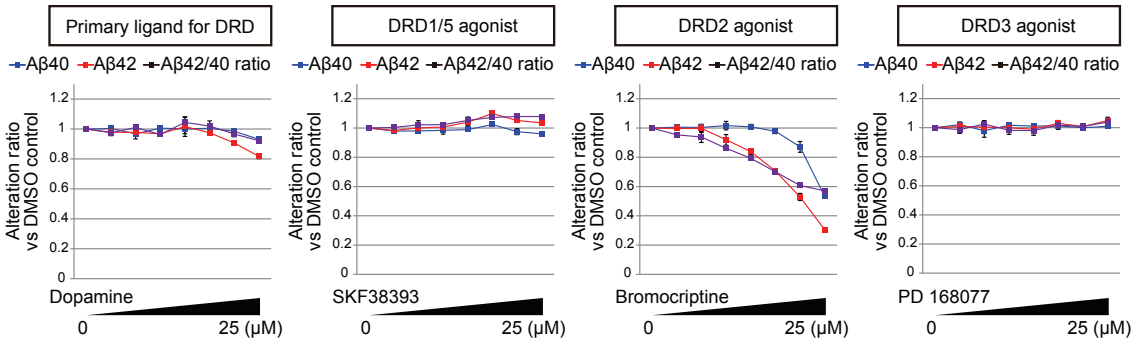

D

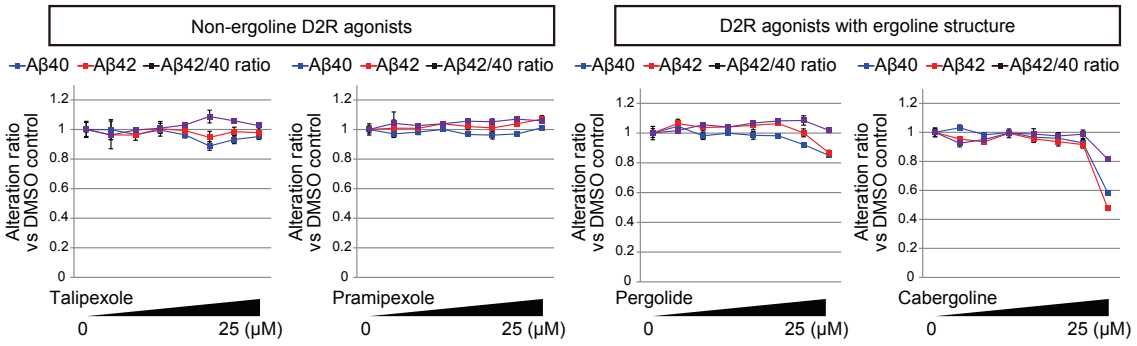

E

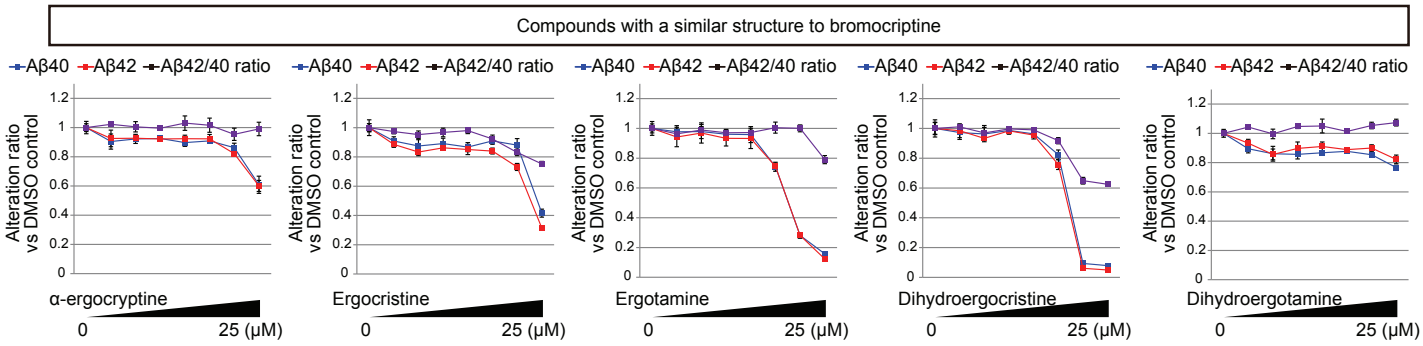

Supplementary Figure S4. Chemical-strugcture-based prioritization and the importance of ergoline structure to modify Aβ metabolsim, Related to Figure 4

(A) Schema of the second-step screening and chemical clustering to prioritize hit compounds. (B) Screening summary using pharmaceutical compounds. (*1) "Screen hits", means the selected compounds after both the first- and second-step screenings. (*2) "Dose-dependency", compounds with a clear dose-dependent change of anti-Aβ effects. (*3) "Toxic hits", compounds that caused neural toxicity at concentrations of 5–25 μM, and were excluded from the final hits. (C) ELISA quantification of Aβ species altered by adding stimulants of dopamine receptor (DRD), including dopamine (primary ligand for DRD), SKF38393 (DRD1/5 agonist), bromocriptine (DRD2 agonist), and PD 168077 (DRD3 agonist). Plots show the results of serial 5-fold dilutions ranging from 1.6 nM to 25 μM of the respective compounds. Data represent mean ± SD (n = 3 for each concentration). (D) ELISA quantification of Aβ species, altered by adding DRD2 agonists that do or do not include the ergoline structure. Plots show the results of serial 5-fold dilutions ranging from 1.6 nM to 25 μM of the respective compounds. Data represent mean ± SD (n = 3 for each concentration). (E) ELISA quantification of Aβ species, altered by adding compounds with a similar structure to bromocriptine. Plots show the results of serial 5-fold dilutions ranging from 1.6 nM to 25 μM of the respective compounds. Data represent mean ± SD (n = 3 for each concentration).

Fig. S5

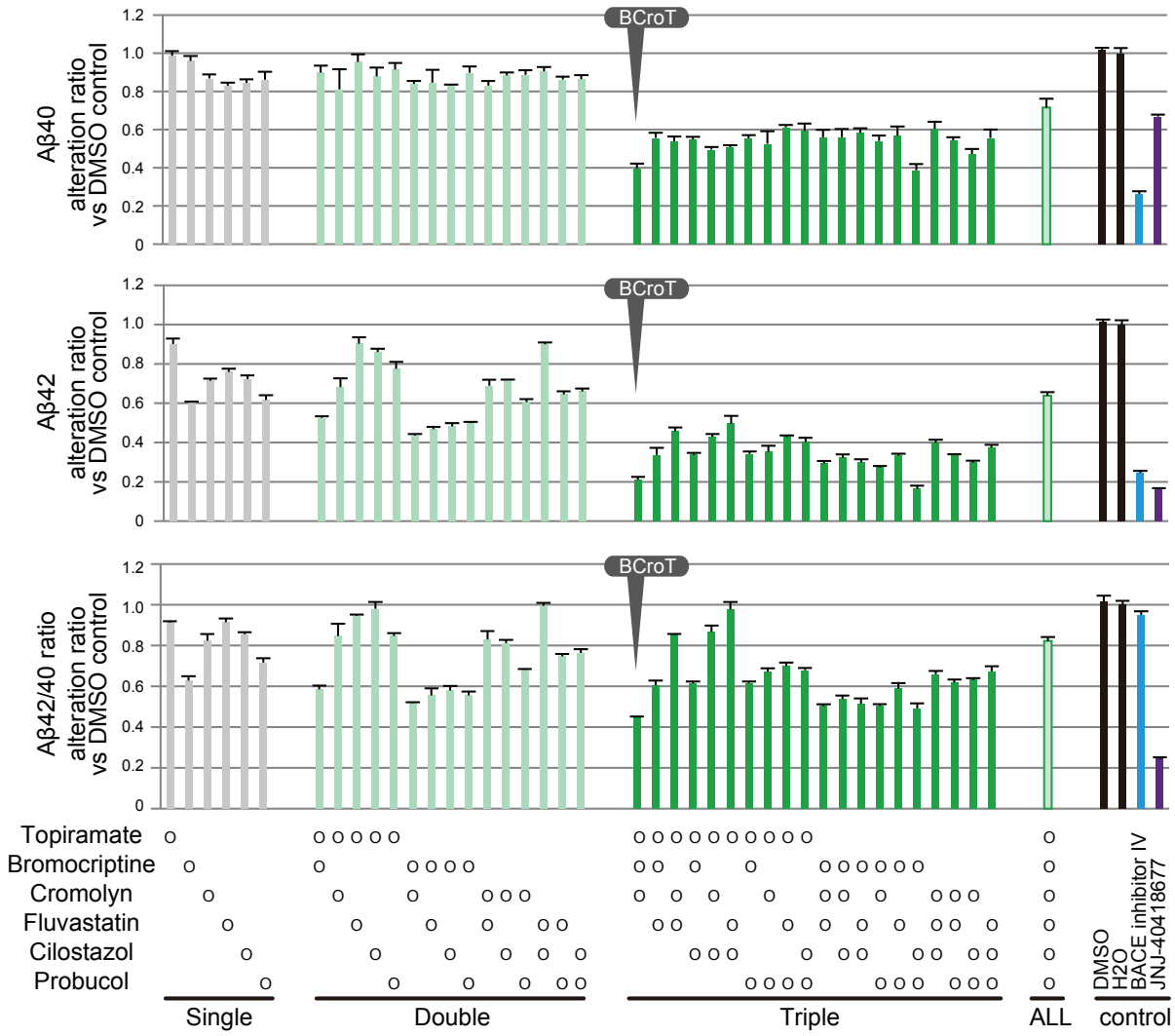
Aβ40 alteration ratio vs DMSO control
Aβ42 alteration ratio vs DMSO control
Aβ42/40 ratio alteration ratio vs DMSO control
BCroT
1.2
1.0
0.8
0.6
0.4
0.2
0
Topiramate
Bromocriptine
Cromolyn
Fluvastatin
Cilostazol
Probucol
Single
Double
Triple
ALL
DMSO
H2O
BACE inhibitor IV
JNJ-40418677
control

Supplementary Figure S5. Round-robin analysis of six lead compounds highlighted the best anti-Aβ cocktail, Related to Figure 5

Alteration of Aβ levels by adding lead compounds in single-, double-, triple-, or all-combinations manner. Concentration of each compound was 1 μM. DMSO (0.1% v/v) or H_2O (0.1% v/v) was used as negative control. BSI IV (1 μM) and JNJ-40418677 (1 μM) were used as a positive control of β–secretase inhibitor and γ–secretase modulator, respectively. BCroT, which showed the highest potency to reduce Aβ, is indicated by the grey speech balloons. (BCroT: combination of bromocriptine, cromolyn, and topiramate).

Fig. S6

A

iPSCs : DAPI TRA1-60 NANOG

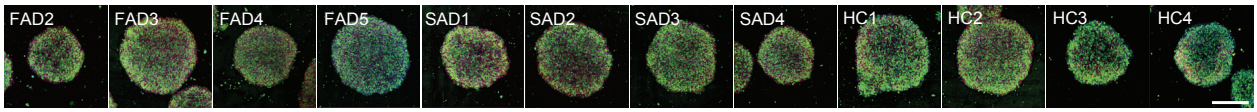

B

iPSC-derived cortical neurons, day8: DAPI MAP2 SATB2

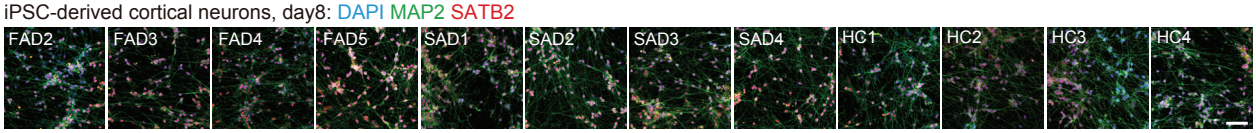

C

iPSC-derived cortical neurons, day8: DAPI VGLUT1 TBR2

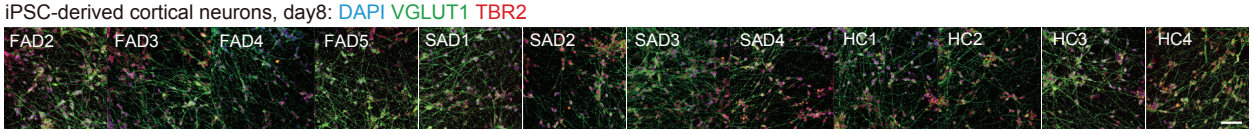

D

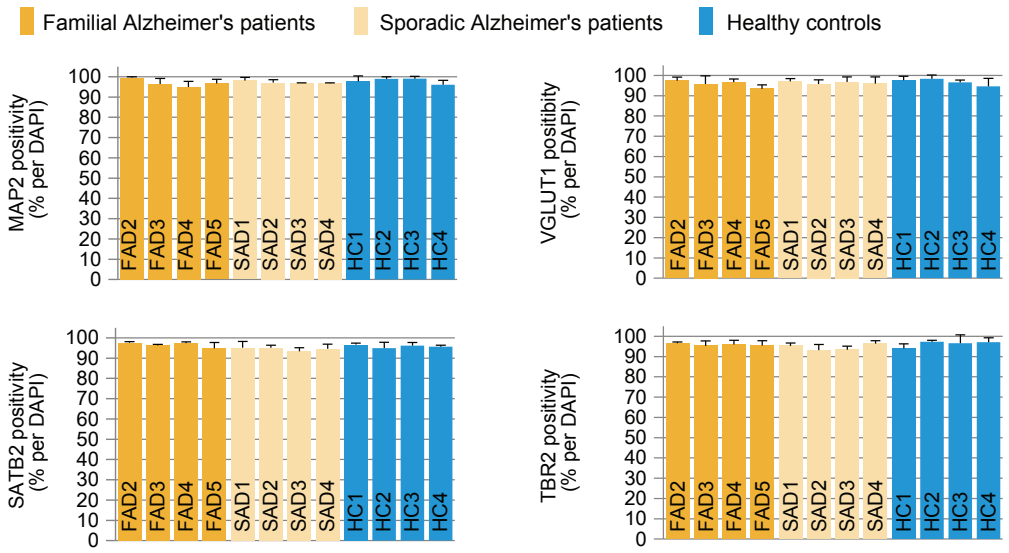

Supplementary Figure S6. Characterization of iPSCs and differentiated cortical neurons, originated from multiple individuals for *in vitro* trial, Related to Figure 6

(A) Generated iPSC clones expressed pluripotency markers TRA1-60 (green) and NANOG (red). Scale bar = 200 μm. Day 8 FAD1-neurons expressed excitatory cortical neuron markers; MAP2 (green) and SATB2 (red) (B), and VGLUT1 (green) and TBR2 (red) (C). Scale bars = 200 μm. (D) Purity of day 8 neurons. Data represent mean ± SD (n = 3 for each clone)

Drug	*in vivo or vitro*	Patients or Models to treat	Effect	Effective concentration, used in experiments	Evidence of mechanism	Reference
Bromocriptine	-	—	N.A.	N.A.	N.A.	N.A.
Cilostazol	*vitro*	Neuro2A cells with APPswedish O.E.	supress Aβ	10-30 μM	increased ADAM10, α-secretase via SIRT1-coupled retinoic acid receptor-β activation	J Neurosci Res. 2014;92(11):1581-90.
Cilostazol	human	MCI patients	ameliorate decrease in MMSE score	130 ± 16 mg/day, p.o.	N.A.	Psychogeriatrics. 2013;13(3):164-9.
Cilostazol	*vivo*	Intracerebroventricular injection of Aβ25–35 in C57BL/6J mice	decrease Aβ deposition decrease phosphorylated Tau and inflammation ameliorate impairment of spatial learning and memory	10 or 20 mg/kg, p.o.	decrease ApoE-mediated Aβ aggregation independent of NEP, IDE	Biochem Biophys Res Commun. 2011;408(4):602-8.
Cilostazol	*vivo*	Intracerebroventricular injection of Aβ25–35 in C57BL/6J mice	ameliorate impairment of working memory	30 or 100 mg/kg, p.o.	ameliorate oxidative stress via MDA	Br J Pharmacol. 2010;161(8):1899-912.
Cilostazol	human	moderate Alzheimer's disease patients	ameliorate decrease in MMSE score	100 mg/day, p.o.	N.A.	Am J Geriatr Psychiatry. 2009;17(4):353-4.
Cilostazol	*vitro*	Neuro2A cells with APPswedish O.E.	decrease phosphorylated Tau	10-30 μM	ameliorate increase of P300 and GSK3β p-Tyr216	J Neurosci Res. 2014;92(2):206-17.
Cilostazol	human	MCI patients	suppress cognitive decline	139 mg/day, p.o.	N.A.	Psychogeriatrics. 2013;13(3):164-9.
Cromolyn	*vivo*	Tg APPswedish / PSEN1 delta E9 mice	decrease TBS-soluble Aβ to 50% no effect on insoluble Aβ nor plasma Aβ	1.05 - 3.15 mg/kg, i.p.	promote microglial Aβ clearance	J Biol Chem. 2015;290(4):1966-78.
Fluvastatin	*vivo*	C57BL/6J mice or Tg APP swedish (APP23) mice	decrease Aβ and APP-CTF	5 mg/kg, in diet admixture	enhance trafficking of APP-CTFs from endosomes to lysosomes increase Aβ clearance from the brain through up-regulating LRP1	J Biol Chem. 2010;285(29):22091-102.
Fluvastatin	*vivo*	Intracerebroventricular injection of Aβ40 in wild-type mice	decrease loss of forebrain neuron ameliorate impairment of spatial learning and memory no effect on NEP nor IDE activity	5 mg/kg	reduction of oxidative stress	Int J Mol Med. 2008;21(5):531-7.
Probucol	human	Alzheimer's disease patients with ApoE4	ameliorate decrease in ADAS-Cog score decrease phosphorylated-Tau in CSF	0.5 g/day, p.o.	increase serum and CSF ApoE	Neurobiol Aging. 2014;35 Suppl 2:S3-10.
Probucol	*vivo*	primary neuron of Tg APP swedish / Indiana (J-20) mice	improve synaptic activity	10 μM	decrease Cyclophilin D-dependent mitochondrial oxidative stress	Biochim Biophys Acta. 2014;1842(12 Pt A):2517-27.
Probucol	*vivo*	C57BL/6J mice with high-fat feeding	decrease Aβ deposition of intestine decrease phosphorylated Tau and inflammation ameliorate impairment of spatial learning and memory	30 mg/kg, in diet admixture	decrease apo B secretion	Lipids. 2012;47(1):27-34.
Probucol	human	moderate Alzheimer's disease patients	decreased CSF-Aβ	1 g/day, p.o.	N.A.	Trends Mol Med. 2003;9(3):94-101.
Topiramate	*vivo*	Tg APPswedish / PSEN1 delta E9 mice	reduce amyloid plaques ameliorate behavioral deficits increase APP-CTF no effect on APP-FL, BACE1	20 mg/kg, i.p.	increase Aβ clearance suppress γ-secretase activity	CNS Neurosci Ther. 2013;19(11):871-81.
Topiramate	*vivo*	Intra-hippocampus injection of Aβ40 in wild-type rats	ameliorate Aβ-induced neuron death	20 mg/kg, i.p.	increase Bcl-2 and Survivin decrease Fas, Bax and Caspase-3	Eur Rev Med Pharmacol Sci. 2014;18(6):761-8.

Abbreviations
CTF: C-terminal fragments, IDE: insulin degrading enzyme, i.p.: intraperioneally, MCI: mild cognitive impairment, MDA: malondialdehyde, N.A.: not available, NEP: Neprilysin, O.E.: over expression, p.o.: *per os*

Supplemental Table S1. Previous *in vivo* research on Alzheimer's disease, regarding lead compounds obtained in this study, Related to Figure 5